Bulletin of the Seismological Society of America, Vol. 86, No. 5, pp. 1434–1446, October 1996

Amplification and Differential Motion due to an Antiplane 2D Resonance in the Sediment Valleys Embedded in a Layer over the Half-Space

by Peter Moczo, Peter Labák, Jozef Kristek, and Franta Hron

Abstract We investigate an antiplane 2D resonance in a certain class of the sedimentary structures using the finite-difference modeling. Our models are derived from the realistic local geologic conditions beneath the colosseum in Rome and are significantly different from those investigated in the previous theoretical articles on a 2D resonance. They include a trough at the bottom of the horizontal surface layer as well as relatively deep sediment valleys embedded in a single layer over the half-space.

We present the finite-difference algorithm for *SH* waves on a combined ($h \times h$ and $2h \times 2h$) rectangular grid. Although being simple, the algorithm allowed us to save up to 75% of the grid points compared with the regular grid $h \times h$ that would cover the same computational region.

A 2D resonance may develop in the valleys that do not satisfy Bard and Bouchon's existence condition.

A simple trough at the bottom of the horizontal surface layer can give rise to the fundamental mode of a 2D resonance whose frequency, spectral amplification, and the maximum time-domain differential motion are very close to those in the closed sediment valley.

Our results confirm that the resonance phenomenon is quite robust and that it is to be expected in many configurations of sediment valleys or basins.

Introduction

In the article by Moczo *et al.* (1995), an *SH* seismic response of the geologic structure beneath the colosseum in Rome, Italy, was numerically investigated. A 2D resonance was observed for a particular model of a relatively deep sediment-filled valley that did not satisfy Bard and Bouchon's (1985) existence condition. Moreover, the resonance exhibited certain interesting unexpected features. Since these findings were related to realistic geologic conditions and may have certain implications for the site-effect estimations in earthquake engineering practice, we have concluded that they deserve more investigation. This article aims to supplement the above-mentioned article and presents the results of a parametric study for a certain class of simple models motivated by the realistic geologic conditions beneath the colosseum in Rome.

Resonance in relatively deep two- or three-dimensional sediment-filled valleys was investigated in several theoretical articles. A pioneer study by Bard and Bouchon (1985) addressed the experimental observations made by Tucker and King (1984) and King and Tucker (1984). It was then followed by Bard and Gariel (1986), Jiang and Kuribayashi (1988), Rial (1989), Mossessian and Dravinski (1990), Ohori *et al.* (1990), Ling and Rial (1990), Rial *et al.* (1991, 1992), Rial and Ling (1992), Ling and Rial (1994), Zhou and Dravinski (1994), and Wirgin (1995). Here we do not review results of these studies because a concise review is given in the article by Zhou and Dravinski (1994), and a detailed critical analysis of the previous investigations is given in the recent theoretical article by Wirgin (1995). Studies by Rial and his co-workers as well as the study by Wirgin provide a systematic deeper insight into the physics of the resonant phenomena. Later we will compare some of our results with those obtained by Bard and Bouchon and Rial and his co-workers.

In all the above-mentioned articles, the medium, in which the sediment valley was embedded, was either elastic/viscoelastic homogeneous or rigid. In this article, as well as in the article by Moczo *et al.* (1995), a horizontal layer in the valley surroundings is considered.

Problem Formulation

We consider as a basic model a relatively deep sediment-filled valley embedded in a medium with a horizontal surface layer (see Fig. 1). The geometry of the valley-basement interface is given by a parabola $z = ax^2 + bx + c$,

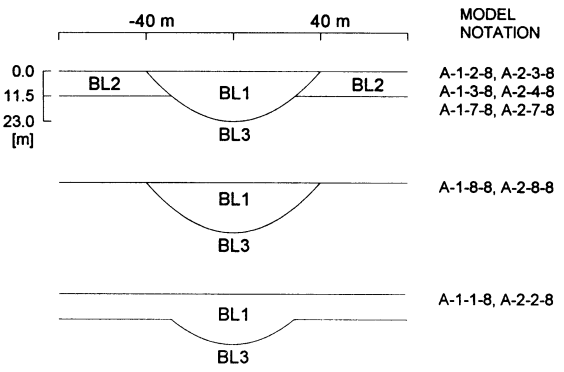

MECHANICAL PARAMETERS

Model	Velocity $\beta[m/s]$ Block			Density $[kg/m^3]$ Block			Quality factor Block		
	BL1	BL2	BL3	BL1	BL2	BL3	BL1	BL2	BL3
A-1-1-8									
A-1-2-8		200			1900			40	
A-1-3-8	100	300	800	1800	1900	2050	10	40	100
A-1-7-8		700			1900			40	
A-1-8-8									
A-2-2-8									
A-2-3-8		300			1900			40	
A-2-4-8	200	400	800	1800	1900	2050	10	40	100
A-2-7-8		700			1900			40	
A-2-8-8									

Figure 1. Geometry and mechanical parameters of the basic valley model and its modifications. The valley is 80-m wide at the free surface and 23-m deep in the center. The equivalent shape ratio (E.S.R.) is 0.4. A-1-*-* denote the higher-contrast models; A-2-*-* denote the lower-contrast models.

where coefficients a, b, and c are determined from the maximum sediment thickness and total width at the free surface. The valley shape ratio, i.e., the ratio of the maximum sediment thickness h to the total width over which the sediment thickness is larger than $h/2$, is equal to 0.4. Since the model is derived from that investigated in the article on the Roman Colosseum, we consider the valley that is 80-m wide at the surface and 23-m deep at the center.

The thickness of the surface layer is $h/2$ (i.e., 11.5 m). The velocity of shear waves inside the valley is either 100 or 200 m/sec, while that in the basement is 800 m/sec in all considered model variations. The velocity in the layer is larger than that in the valley but smaller than the velocity in the basement. The density and quality factor values are given in Figure 1. The six basic model variations are labeled A-1-2-8, A-1-3-8, A-1-7-8 and A-2-3-8, A-2-4-8, A-2-7-8 (see Fig. 1).

Besides the basic model, its two extreme modifications are investigated as well. In the first of them, the layer material is the same as in the underlying basement (the A-1-8-8 and A-2-8-8 models shown in Fig. 1). In the second modification, the layer material is the same as in the valley (A-1-1-8 and A-2-2-8), which gives, in fact, a model of a trough at the bottom of the horizontal layer.

In this way, we have the higher-contrast models (A-1-*-8) and the lower-contrast models (A-2-*-8).

The valley is subjected to a plane *SH* wave incident vertically from below. We compute translational and differential motions at the free surface of the valley and its vicinity.

A Finite-Difference Algorithm on a Combined Rectangular Grid for *SH* Waves

In order to solve the above-formulated problem, we use the finite-difference method. The well-known advantages of the finite-difference method are its applicability to complex realistic media, relative simplicity, and the fact that it is easy to implement in the computer codes. One of its disadvantages is the relatively large computer memory requirement.

Here we present a simple algorithm for *SH* waves on a combined rectangular grid that is applicable in case the near-surface inhomogeneity is underlain by a homogeneous material. Although being simple, the algorithm allowed us to save up to 75% of the grid points compared with the regular grid that would cover the same computational region. The test computations performed for the selected models showed that the absolute value of the difference between the time-domain response obtained on the combined grid and that on the equivalent regular grid was below 1%.

Equations of Motion

We consider an attenuating medium in which the attenuation is implemented according to Emmerich and Korn (1987). The rheology of the medium is then that of a generalized Maxwell body.

Let the computational region be an xz-plane and the shear modulus μ and the density ρ dependent on both x- and z-coordinates. Then the y-component of the displacement vector $v(x, z, t)$ is governed by the equations (Moczo and Bard, 1993)

$$\rho\ddot{v} = (\mu v_x)_x + (\mu v_z)_z - \sum_{j=1}^{n} \xi_j^v, \tag{1}$$

$$\dot{\xi}_j^v + \omega_j \xi_j^v = \omega_j[(\mu Y_j^\mu v_x)_x + (\mu Y_j^\mu v_z)_z], \quad j = 1,\ldots,n. \tag{2}$$

In a homogeneous medium, μ and ρ are constants, and the equations become simpler:

$$\rho\ddot{v} = \mu(v_{xx} + v_{zz}) - \sum_{j=1}^{n} \xi_j^v, \tag{3}$$

$$\dot{\xi}_j^v + \omega_j \xi_j^v = \omega_j \mu Y_j^\mu (v_{xx} + v_{zz}), \quad j = 1,\ldots,n. \tag{4}$$

Here, ω_j ($j = 1, \ldots, n$) are the relaxational (angular) frequencies. The coefficients Y_j^μ ($j = 1, \ldots, n$) are obtained from the system of equations

$$\sum_{j=1}^{n} \frac{\omega_j \tilde{\omega}_k + \omega_j^2 \tilde{Q}_\beta^{-1}(\tilde{\omega}_k)}{\tilde{\omega}_k^2 + \omega_j^2} Y_j^\mu = \tilde{Q}_\beta^{-1}(\tilde{\omega}_k), \quad k = 1, \ldots, 2n - 1,$$

where $\tilde{Q}_\beta(\tilde{\omega}_k)$ are the desired values of the quality factor at the specified frequencies $\tilde{\omega}_k$. In the inhomogeneous medium, $\tilde{Q}_\beta$ also depends on x- and z-coordinates.

The coefficients Y_j^μ have the following meaning: μY_j^μ is the elastic modulus, and $\mu Y_j^\mu/\omega_j$ is the viscosity of the jth classical Maxwell body. n classical Maxwell bodies are connected in parallel together with a single spring with the elastic modulus equal to $\mu(1 - \sum_{j=1}^{n} Y_j^\mu)$.

Finite-Difference Schemes on the Rectangular Grids

The computational region is covered by a combined rectangular grid shown in Figure 2. The regular grid $h \times h$ is used for the inhomogeneous part of the model, while the grid $2h \times 2h$ is employed for the homogeneous one. Equations (1) through (4) can be solved by the finite-difference schemes similar to those in Moczo and Bard (1993):

$$\begin{aligned} v_{il}^{m+1} &= 2v_{il}^m - v_{il}^{m-1} \\ &\quad + \frac{\Delta^2 t}{\rho_{il}} \left[L_{xx}(\mu; v) + L_{zz}(\mu; v) \right. \\ &\quad \left. + \frac{1}{2} \sum_{j=1}^{n} (\xi_{j,il}^{v,m+1/2} + \xi_{j,il}^{v,m-1/2}) \right], \end{aligned} \tag{5}$$

$$\begin{aligned} \xi_{j,il}^{v,m+1/2} &= \frac{2 - \omega_j \Delta t}{2 + \omega_j \Delta t} \xi_{j,il}^{v,m-1/2} \\ &\quad + \frac{2\omega_j \Delta t}{2 + \omega_j \Delta t} [L_{xx}(\mu Y_j^\mu; v) + L_{zz}(\mu Y_j^\mu; v)], \end{aligned} \tag{6}$$

$j = 1, \ldots, n$. Here, Δt is the time step, v_{il}^m is the discrete approximation of the displacement $v(x_i, z_l, t_m)$, and $\xi_{j,il}^{v,m}$ is the discrete approximation of the function $\xi_j^v(x_i, z_l, t_m)$.

In an inhomogeneous medium, on the grid $h \times h$, the L_{xx} and L_{zz} operators have the form

$$L_{xx}(a; f) = \frac{1}{h^2} [a_{il}^H (f_{i+1l}^m - f_{il}^m) - a_{i-1l}^H (f_{il}^m - f_{i-1l}^m)] \tag{7}$$

and

$$L_{zz}(a; f) = \frac{1}{h^2} [a_{il}^V (f_{il+1}^m - f_{il}^m) - a_{il-1}^V (f_{il}^m - f_{il-1}^m)], \tag{8}$$

where a_{il}^H and a_{il}^V are the horizontal and vertical effective parameters:

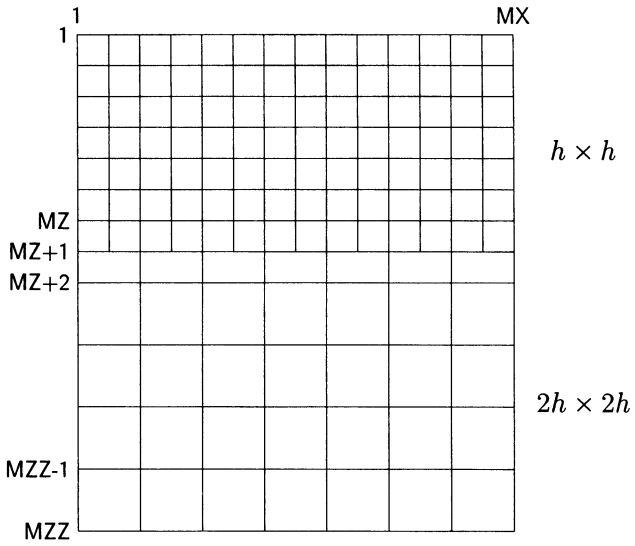

Figure 2. Combined rectangular grid used in the finite-difference computations. The grid $h \times h$ covers the inhomogeneous part of a medium, while the grid $2h \times 2h$ is used for the homogeneous basement.

$$a_{il}^H = h \left(\int_{x_i}^{x_{i+1}} \frac{dx}{a(x, z_l)} \right)^{-1}, \quad a_{il}^V = h \left(\int_{z_l}^{z_{l+1}} \frac{dz}{a(x_i, z)} \right)^{-1}.$$

In a homogeneous medium, on the grid $2h \times 2h$, the L_{xx} and L_{zz} operators are

$$L_{xx}(a; f) = \frac{a}{4h^2} (f_{i+2l}^m - 2f_{il}^m + f_{i-2l}^m)$$

and

$$L_{zz}(a; f) = \frac{a}{4h^2} (f_{il+1}^m - 2f_{il}^m + f_{il-1}^m).$$

Finite-Difference Schemes at the Contact of the $h \times h$ and $2h \times 2h$ Grids

There are two types (say A and B) of the grid points at the transition grid row (labeled $MZ + 1$ in Fig. 2). The two types of grid points are shown in Figure 3.

For the A-type grid point, the schemes (5 and 6) can be used with the operators

$$L_{xx}(a; f) = \frac{a}{h^2} (f_{i+1l}^m - 2f_{il}^m + f_{i-1l}^m) \tag{9}$$

and

$$L_{zz}(a; f) = \frac{a}{h^2} (f_{il+1}^m - 2f_{il}^m + f_{il-1}^m). \tag{10}$$

In order to avoid interpolation that would decrease the order of the finite-difference approximation, the B-type grid

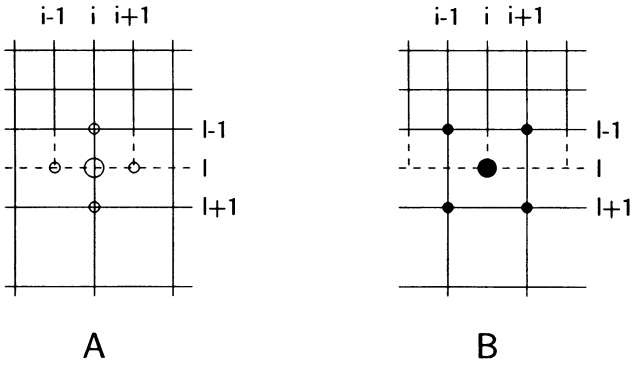

Figure 3. Two types of the grid points at the contact of the grids $h \times h$ and $2h \times 2h$. A special finite-difference scheme is used for the B type in order to avoid interpolation that would decrease the order of approximation.

point requires a special scheme. As it is clear from equations (3) and (4), it is possible to approximate directly the sum of both derivatives $v_{xx} + v_{zz}$. The corresponding operator is

$$L_{xx,zz}(f) = \frac{1}{2h^2}\,(f^m_{i+1l+1} + f^m_{i-1l+1} + f^m_{i+1l-1} + f^m_{i-1l-1} - 4f^m_{il}).$$

The approximation is of the second order as are the approximations (7) and (8). Then we will have $\mu L_{xx,zz}(v)$ instead of $L_{xx}(\mu; v) + L_{zz}(\mu; v)$ in scheme (5). Similarly, $\mu Y^\mu_j L_{xx,zz}(v)$ will replace $L_{xx}(\mu Y^\mu_j; v) + L_{zz}(\mu Y^\mu_j; v)$ in scheme (6).

Although our grid combines the grids $h \times h$ and $2h \times 2h$, its use is not restricted to the cases when the velocity in the homogeneous basement (β) is twice or more larger than the minimum velocity in the inhomogeneous medium ($\beta_{\min}$). The combined grid can be used even in the case of $1 < \beta/\beta_{\min} < 2$. It is just necessary to apply the sampling criterion in the homogeneous basement first in order to determine the grid spacing of the grid $2h \times 2h$.

Numerical Computations

Due to the symmetry of both the model and wave field, only a right half of the model was covered by a combined spatial grid. The total computational area was 420-m long and 199-m deep for all models, except the model of a trough at the bottom of the horizontal layer. For the latter, the area was 2508-m long and 199-m deep. The relatively long area was used in order to prevent any contamination due to laterally propagating diffracted waves and imperfection of the Reynolds (1978) transparent boundary.

The parameters of the combined spatial grid (see Fig. 2) were $MX = 841$ (5017 for the trough model), $MZ = 100$, $MZZ = 250$, and $h = 0.5$ m. The time step was 0.00036 sec. The theoretical accuracy of the finite-difference computations was at least up to 15 Hz.

A Gabor wavelet was used as a time function of the incident wave. It is defined by

$$s(t) = e^{-(\omega_p(t-t_s)/\gamma)^2} \cos(\omega_p(t - t_s) + \psi),$$

with

$$\omega_p = 2\pi f_p, \quad t_s = 0.45\gamma/f_p, \quad \text{and } t \in \langle 0, 2t_s\rangle.$$

The free parameters make it possible to simulate signals with desirable amplitude spectra.

A "δ-like" input signal with broad amplitude spectrum was used to obtain the pseudoimpulse responses. Then the Fourier transfer function for each site was obtained by dividing the Fourier spectrum of the local pseudoimpulse response by the Fourier spectrum of the "δ-like" signal.

Results

The 2D Resonance. Before we show results for models with a surface layer, let us recall what is meant by a 2D resonance in a simple valley model with the homogeneous basement—e.g., in the A-1-8-8 model. Figure 4 shows the time-domain representations of the fundamental antiplane shear mode (a) and the first higher symmetric mode (b). They are obtained as the time-domain responses to the Gabor wavelets with relatively narrow amplitude spectra centered around resonant frequencies 1.25 and 2.41 Hz, respectively. In the case of the fundamental mode, we can see a characteristic in-phase motion of a major part of the valley surface with the maximum amplitude at the valley center. The first higher mode exhibits two nodes at which the surface motion changes its sign. Spectral amplifications due to both resonant modes will be shown later.

The Existence Condition. We have found that at least the fundamental and first higher modes of a 2D resonance can develop inside the valleys in all investigated models with a surface horizontal layer, i.e., in the models A-1-2-8, A-1-3-8, A-1-7-8 and A-2-3-8, A-2-4-8, A-2-7-8. Let us compare our valley models with those that satisfy Bard and Bouchon's (1985) existence condition for the valleys embedded in a homogeneous basement. The condition is represented by a curve in Figure 5. If the valley of a certain velocity contrast and a shape ratio appears above the curve, the 2D resonance of the valley takes place. If the valley appears below the curve, an induced surface-wave lateral propagation and a vertical 1D resonance should take place in the valley. (Bard and Bouchon obtained their delimiting curve with sine-shaped valleys, but, as they noted, the curve is valid for any valley shape provided that the real shape ratio, i.e., the maximum sediment thickness to the valley half-width, be replaced by an equivalent shape ratio, as was de-

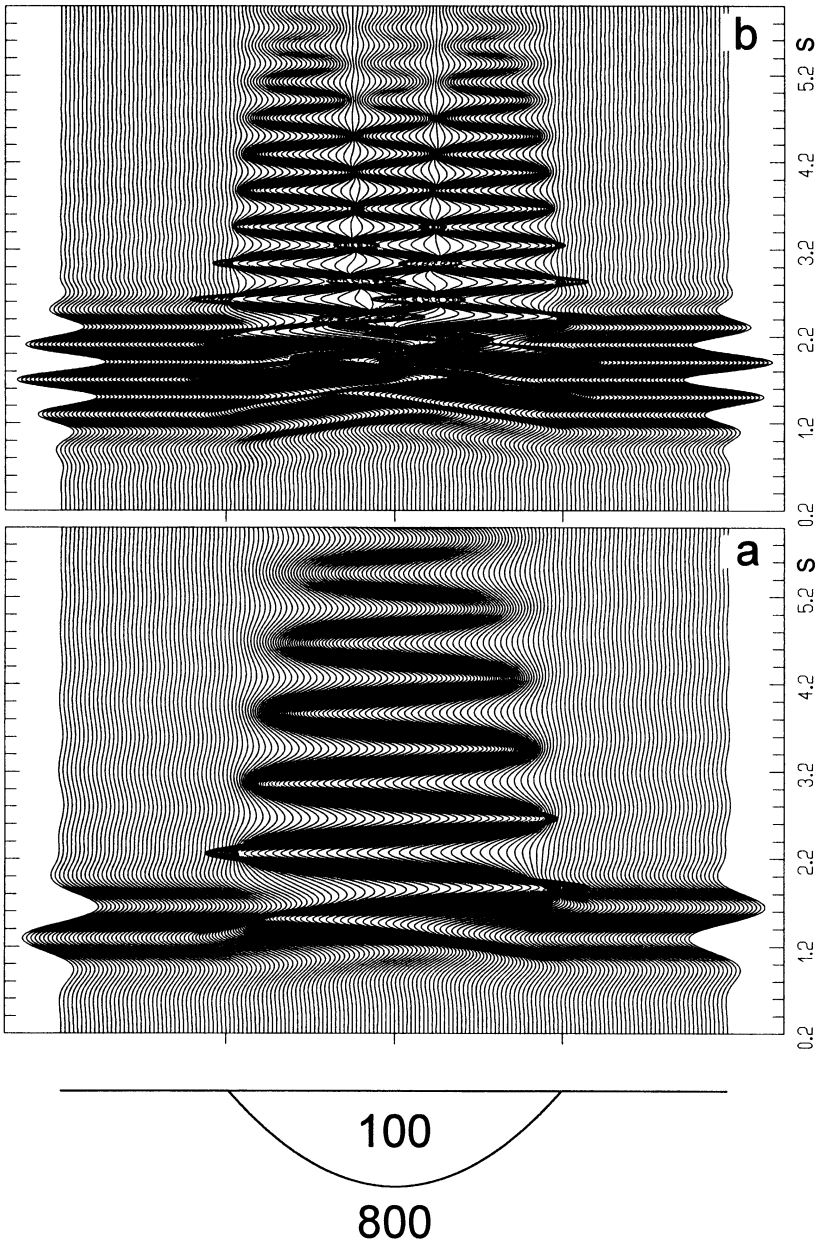

Figure 4. The surface motion due to (a) the fundamental antiplane shear mode and (b) the first higher symmetric mode of the 2D resonance in the valley model A-1-8-8. The Gabor wavelets with parameters $\gamma = 4, f_p = 1.25$ Hz, $\psi = \pi/2$ and $\gamma = 9.5, f_p = 2.41$ Hz, $\psi = \pi/2$, respectively, were used as input signals.

fined in the Problem Formulation section of this article.) As it is shown in Figure 5, the velocity contrasts at the valley-layer interface in the A-1-2-8, A-1-3-8 and A-2-3-8, A-2-4-8 models are well below Bard and Bouchon's existence value. In this sense, the four valley models do not satisfy Bard and Bouchon's condition. Despite this fact, they can give rise to the 2D resonance.

The Effect of the Horizontal Surface Layer. In view of the above finding, it is interesting to see the effect the surface layer may have on a 2D resonance in the valley. To do so, we compare the surface motion in the valley models, which include the horizontal surface layer, with the motion in the valley embedded in a homogeneous medium (i.e., when the layer material is the same as in the underlying basement). Comparison of the fundamental and first higher modes in the lower-contrast models A-2-3-8, A-2-4-8, A-2-7-8 and A-2-8-8 is shown in Figure 6. The left part of the figure shows the spatial variations of the amplification (modulus of the Fourier transfer function) at the resonant frequencies with respect to the incident wave. The right part of the figure shows the spatial variations of the moduli of the differential motion maxima taken over the entire computed time windows of the resonant modes. The differential motion $\partial u/\partial x$ is evaluated as a difference between the translational motions at two adjacent positions (grid points) divided by the corresponding grid spacing (0.5 m).

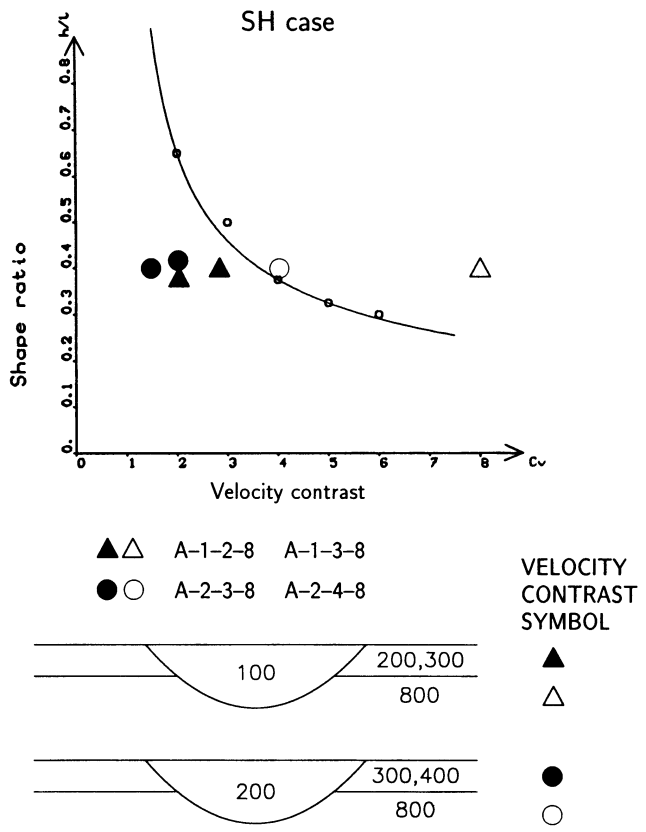

Figure 5. Comparison of the studied valley models with Bard and Bouchon's (1985) existence condition represented by the *shape ratio–velocity contrast* curve. Valleys below the curve should not give rise to a 2D resonance. We observe a 2D resonance in the four valleys shown in the picture despite the fact that the valley-layer velocity contrasts are well below the existence curve.

We can see that the fundamental mode is almost insensitive to the presence of the surface layer and that the first higher mode is only a little bit affected.

A similar comparison for the higher-contrast models A-1-2-8, A-1-3-8, A-1-7-8 and A-1-8-8 is shown in Figure 7. The differences among the surface motions of different valley models are now a little bit larger than in the previous case, but they still remain relatively small.

Let us note that the differential motion in the higher-contrast models is evaluated in the same way as in the lower-contrast models, i.e., using the translational motions at two adjacent grid points separated by the 0.5-m spacing. In this sense, the differential motion is not scaled with respect to the dominant wavelength in the valley. Such an evaluation of the differential motion is reasonable, however, from the earthquake-engineering point of view.

The Effect of the Valley-Basement Velocity Contrast. Figure 8 shows all the lower- and higher-contrast models together. Of course, both groups of models relate to different resonant frequencies since the difference in the valley-basement velocity contrast is given by the velocity inside the valley.

Let us first have a look at the fundamental mode. There is a striking difference between the maximum spectral amplification and differential motion in their relation to the lower- and higher-velocity contrast. As we can see, twice smaller velocity contrast (i.e., 2:8) implies approximately twice (viz., 1.8) smaller spectral amplification compared to that in the higher-contrast (1:8) models. This is not true, however, about the differential motion. The difference in the velocity contrast has only a little influence on the maximum time-domain differential motion: the corresponding ratio between the two maxima is less than 1.2.

One may find this result surprising at first glance. It is, however, easy to understand if we compare the maximum time-domain amplitudes of the fundamental modes at the valley center in the 1:8 and 2:8 cases. If we take the maximum amplitude in the 1:8 case (9.27 cm for a maximum basement displacement of 1 cm) as a reference, the maximum amplitude in the 2:8 case (8.23 cm) is only 11.2% lower. As a consequence, the corresponding difference between the maximum time-domain differential motions is less than 15% (i.e., the ratio between the two values is less than 1.2).

The situation is different in the frequency domain. The spectral amplification includes both the effect of the time-domain amplitudes and the effect of the duration of motion. While the time-domain amplitude of the fundamental mode at the valley center decreases from its maximum to 1/10 of the maximum in 6.3 sec in the 1:8 case, the equivalent decrease in the 2:8 case takes only 2.81 sec (i.e., 2.2 times less). As a consequence, the maximum spectral amplification as well as the maximum differential motion in the frequency domain (i.e., the maximum absolute value of the spatial derivative of the Fourier transfer function) in the 1:8 case are about twice as large as those in the 2:8 case.

The first higher mode behaves in a different manner. Neither the spectral amplification nor the maximum time-domain differential motion is much sensitive to the difference in the valley-basement velocity contrast.

The Effect of the Valley Shape and Shape Ratio. There should be some other parameters to which the differential motion due to both resonant modes and the spectral amplification due to the first higher mode are more sensitive. Let us now consider only the case of the valley embedded in a homogeneous medium and consider, for both the higher- and lower-velocity contrasts, three different valley shape ratios—0.3, 0.4, and 0.5. In the first set of the valley models, we keep the total width at the surface fixed and vary the maximum depth of the valley (Fig. 9). In the second set of the models we keep the maximum depth of the valley fixed and vary the total width at the surface (Fig. 10). We compare the amplification and differential motion due to the resonant

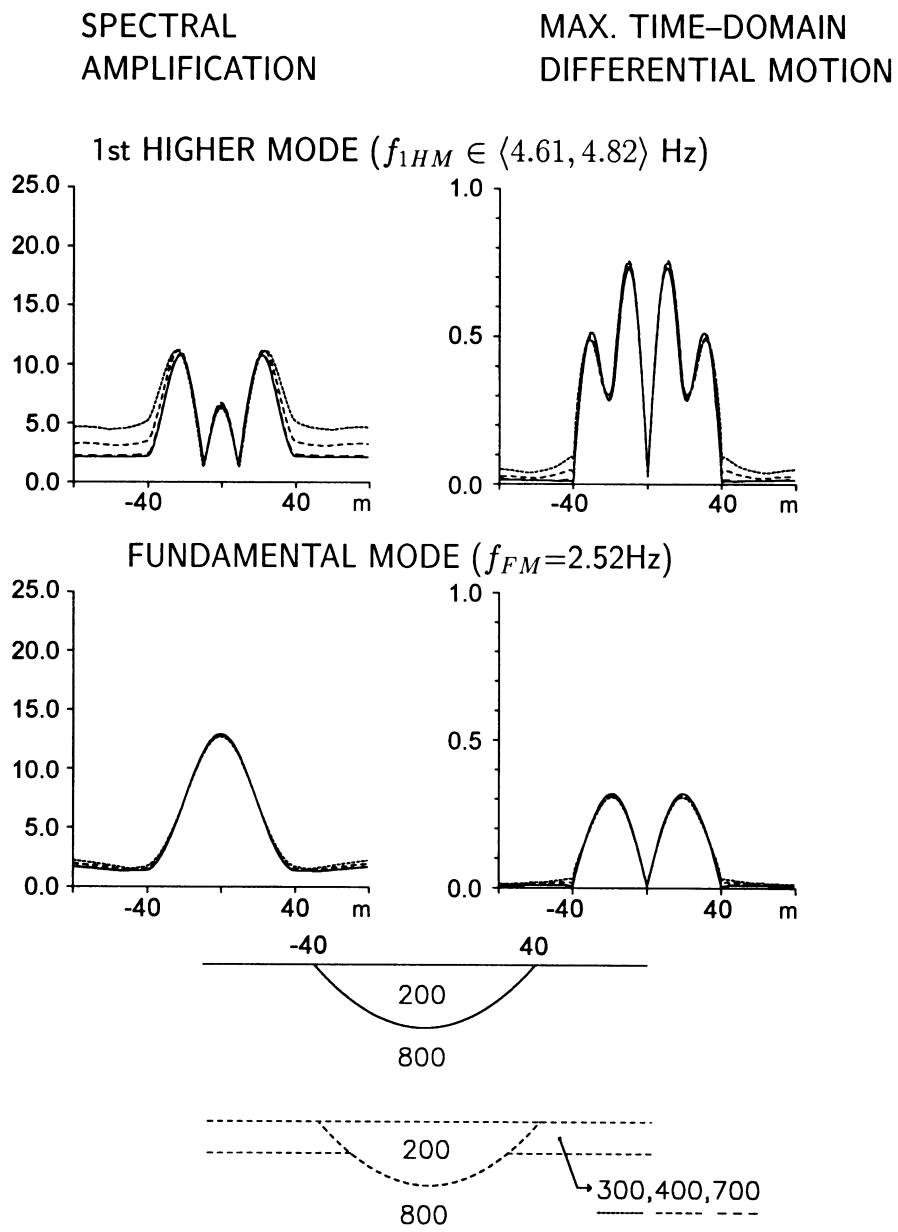

Figure 6. Effect of a horizontal surface layer in the valley surroundings on the spectral amplification and the maximum time-domain differential motion related to the fundamental and first higher modes in the lower-contrast valleys. The values of the differential motion have to be multiplied by 10^{-2} to be scaled for a maximum basement displacement of 1 cm.

modes, keeping in mind, of course, that the corresponding resonant frequencies are different in different valleys since they are determined by the actual valley shape. The computations, including those not shown in the figures, indicate that the spectral amplification due to the first higher mode may be much more sensitive to the valley shape ratio and the shape of the valley than to the valley-basement velocity contrast if the contrast is large enough. This sensitivity is even more pronounced in the case of the differential motion due to both resonant modes.

The Fundamental Mode due to a Trough at the Bottom of the Horizontal Layer. Let us compare two extreme modifications of our basic model of the valley embedded in the medium with a horizontal surface layer. In the first one, the layer material is the same as in the underlying basement, i.e., the valley is embedded in a homogeneous medium. The corresponding models A-1-8-8 and A-2-8-8 have already been included in previous comparisons. In the second modification, the layer material is the same as in the valley (A-1-1-8, A-2-2-8; see Fig. 1). The second modification gives, in

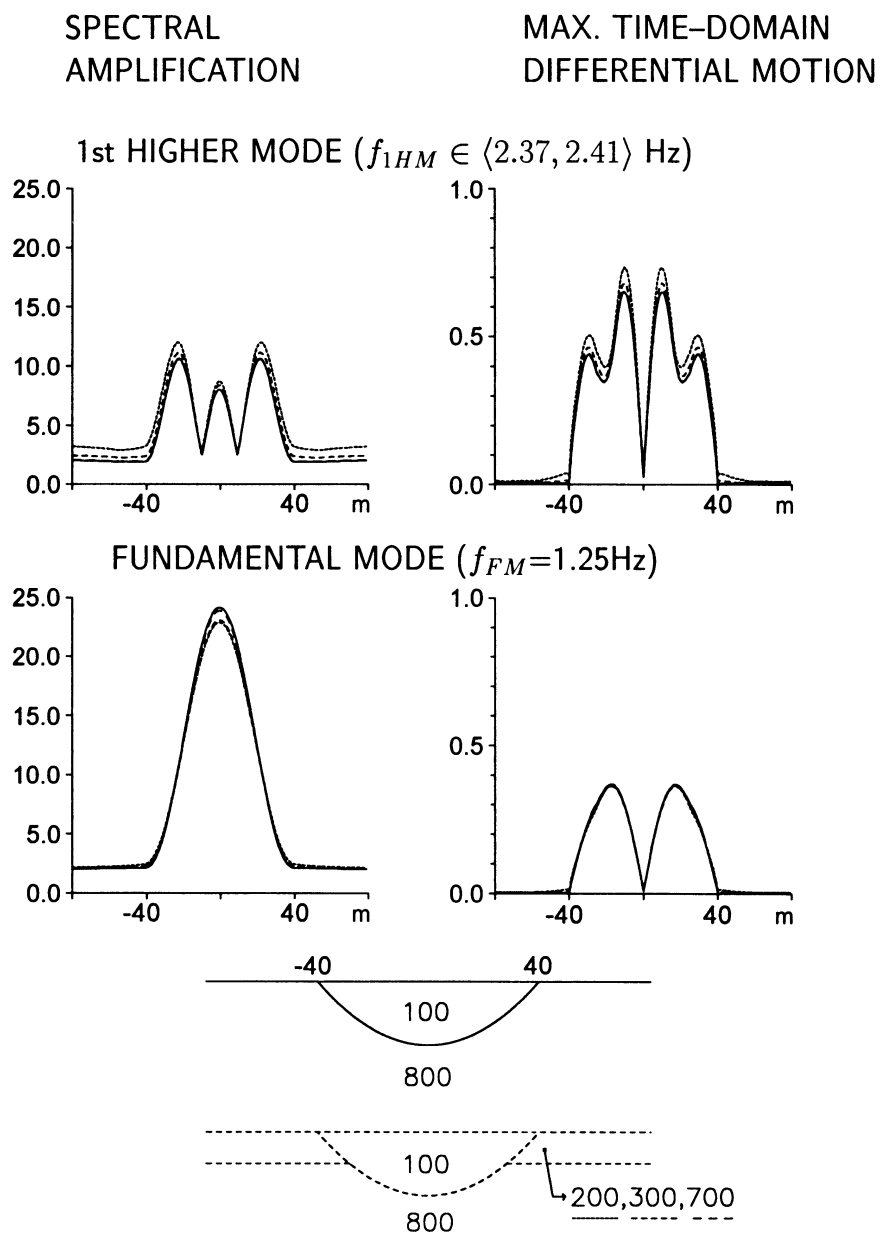

Figure 7. Similar to Figure 6, but for the higher-contrast valleys.

fact, a model of a horizontal layer with a trough at the bottom. As our computations show, the trough can give rise to the fundamental mode of a 2D resonance. Moreover, the resonant frequency, spectral amplification, and maximum time-domain differential motion due to the fundamental mode are very close to those for the closed valley embedded in a homogeneous medium. This is illustrated in Figures 11 and 12. Figure 11 shows a time-domain representation of the resonant modes in both the higher- and lower-contrast trough models. Compare the fundamental mode in the higher-contrast model with that shown in Figure 4a for the closed valley. Figure 12 shows comparison of the corresponding spectral amplifications and differential motions with those for the closed valleys. The resonant frequencies 1.23 and 2.44 Hz in the trough models are very close to the resonant frequencies 1.25 and 2.52 Hz in the closed valleys.

The above results are actually not surprising in view of findings made previously by Bard and Bouchon and Rial and his co-workers. They found that the fundamental mode is confined to the central part of the valley. Rial demonstrated that the fundamental mode, its eigenfrequency and eigenfunction, is determined by a geometry of the central part of the valley. In other words, the absence of lateral bounds of sediments at the free surface in our trough model cannot prevent the fundamental mode to develop.

Let us now compare a resonance in the trough model

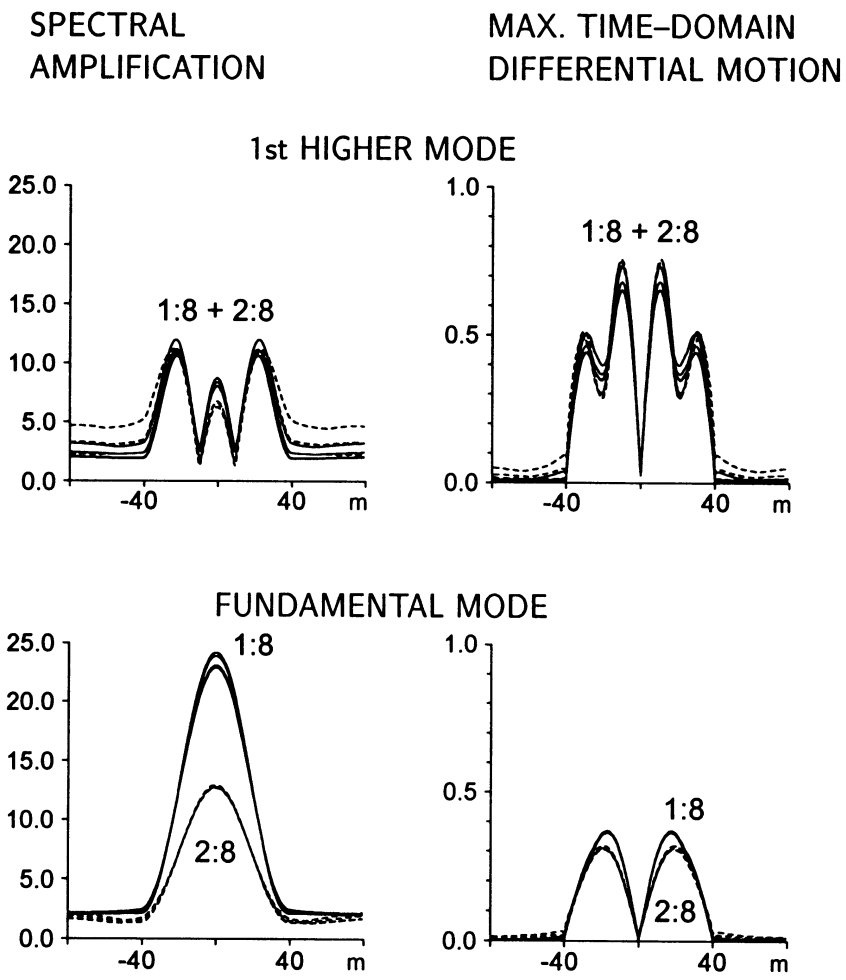

Figure 8. Comparison of the spectral amplifications and the maximum time-domain differential motions in the higher- and lower-contrast valley models shown in Figures 6 and 7.

with a vertical 1D resonance in the surface flat layer whose thickness is equal to the maximum thickness of the sediments in the trough model. The velocity in the layer is 100 m/sec in the higher-contrast case and 200 m/sec in the lower-contrast case. The other parameters are the same as in the trough models. The 1D-resonance frequencies are 0.94 and 1.92 Hz in the higher-contrast and lower-contrast flat layer models, respectively. It is important that in both cases, the resonant frequencies in the trough models are significantly closer to those in the closed valleys than to the 1D-resonance frequencies in the flat layers. This is also true about the corresponding maximum spectral amplifications. In the higher-contrast case, they are 24.2, 22.3, and 11.1 in the closed valley, trough model, and flat layer, respectively. In the lower-contrast case, they are 12.9, 11.5, and 6.8. Another important difference between the trough and flat layer is that there is no differential motion $\partial u/\partial x$ in the flat layer, while that in the trough model is close to the differential motion in the closed valley.

Let us note that the trough at the bottom of the layer does not give rise to the first higher mode. This is understandable since the first higher mode is mainly due to lateral interferences, as was explained by Bard and Bouchon and later demonstrated by Rial and his co-workers.

Conclusions and Earthquake-Engineering Implications

Having been motivated by the realistic local geologic conditions beneath the colosseum in Rome, we have performed a parametric study of an antiplane 2D resonance in a certain class of relatively deep two-dimensional sediment-filled valleys embedded in a single layer over the half-space. We have investigated existence of a 2D resonance, spectral amplification, and a maximum time-domain differential motion at the free surface related to the fundamental and first higher modes. We have shown that an antiplane 2D resonance can develop in the sedimentary structures that are sig-

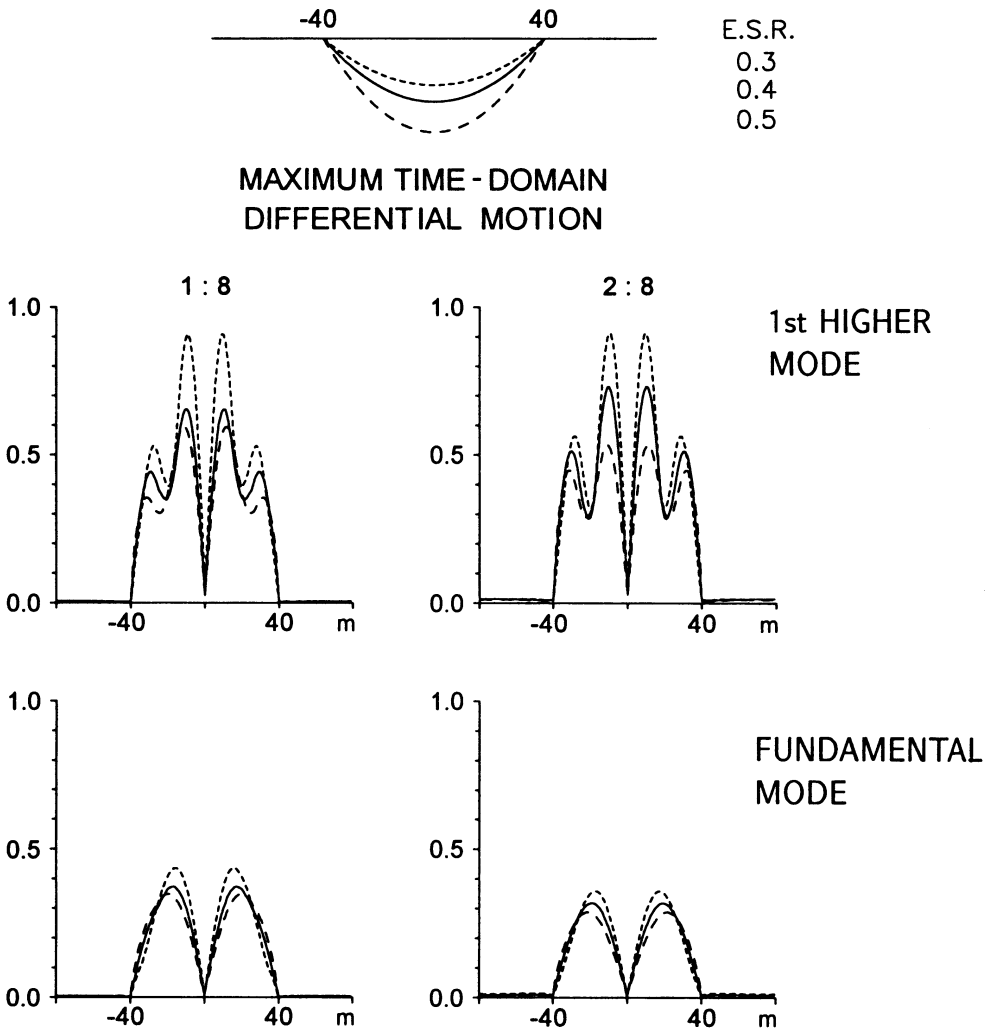

Figure 9. Effect of the valley shape ratio on the maximum time-domain differential motion related to the fundamental and first higher modes in both the higher- and lower-contrast valleys. The values of the differential motion have to be multiplied by 10^{-2} to be scaled for a maximum basement displacement of 1 cm.

nificantly different from those investigated in the previous theoretical studies.

We have presented a finite-difference algorithm on a combined ($h \times h$ and $2h \times 2h$) rectangular grid. The algorithm allowed us to save up to 75% of the grid points compared with the regular grid $h \times h$ that would cover the same computational region.

Based on the results of the performed numerical simulations, we can draw the following conclusions:

a. A 2D resonance can arise in the valleys embedded in a medium with a horizontal surface layer (whose thickness is a half of the maximum valley depth), even in the case when the valley-layer velocity contrast is well below Bard and Bouchon's (1985) existence value. In other words, a 2D resonance can arise in the valleys that do not satisfy Bard and Bouchon's existence condition.

b. The fundamental and first higher modes are not much sensitive to the presence of the surface layer whose thickness is equal to or smaller than half the maximum valley depth and whose shear-wave velocity is larger than that in the valley but smaller than the velocity in the underlying basement.

c. The differential motion due to the fundamental and first higher modes and the spectral amplification due to the first higher mode are more sensitive to the valley shape ratio and the shape of the valley than to the valley-basement velocity contrast if the contrast is high enough.

d. Compared to the maximum spectral amplification, the maximum time-domain differential motion due to the fundamental mode is much less sensitive to the valley-basement velocity contrast. The twice smaller valley-basement velocity contrast implies approximately twice smaller spectral amplification, at the corresponding res-

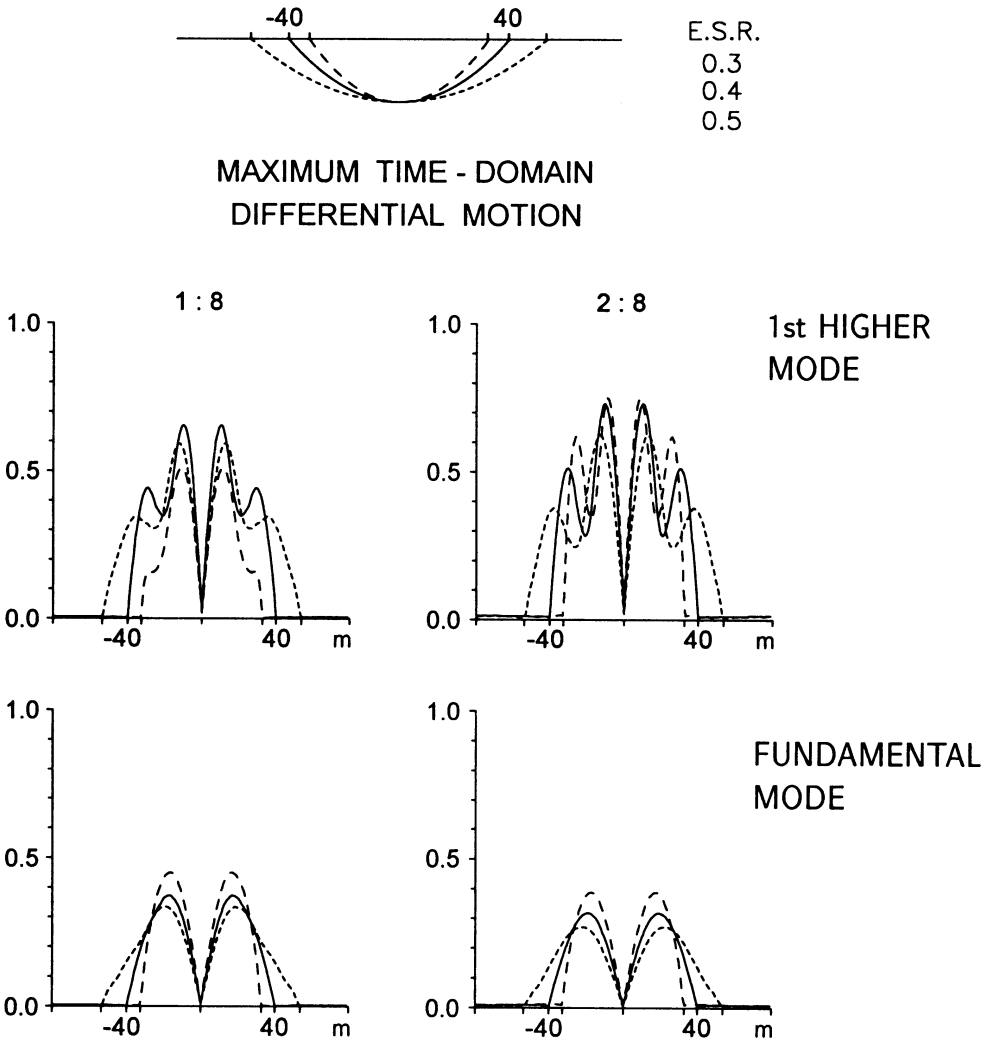

Figure 10. Similar to Figure 9.

onant frequency, but it affects only little the differential motion.

e. A simple trough at the bottom of the horizontal surface sedimentary layer can give rise to the fundamental mode of a 2D resonance whose frequency, spectral amplification, and the maximum time-domain differential motion are very close to those in the closed sediment valley.

It is obvious that it is very important for the seismic hazard assessment and earthquake engineering practice to know under which geologic conditions the significant resonant phenomena can arise. This is especially true if these phenomena are due to the lateral near-surface heterogeneities and cannot be explained by 1D models. We believe that our parametric study, though restricted to the *SH* case, contributes to the knowledge of the local resonant phenomena since the above-mentioned properties of the 2D resonance and its existence in the specific sedimentary structures may not have been obvious without computations such as those in the present study.

Our computations confirm that the resonant phenomenon is to be expected in many configurations of valleys or basins. The likelihood of the resonance is relatively high since the velocity contrast that determines the occurrence of the resonance seems to be the contrast between the sediments and the bedrock below the basin.

Our computations partly confirm predictions made by Rial *et al.* (1991, 1992). They stressed that, generally, the concave upward segments of the sediment-rock boundary can give rise to localized resonances. They link such resonances with observed pockets of damage in several major earthquakes.

In conclusion, we point out to the two indications that are, in our opinion, especially important for an earthquake-engineering practice, namely, that (1) two valleys with very different levels of spectral amplification (at the correspond-

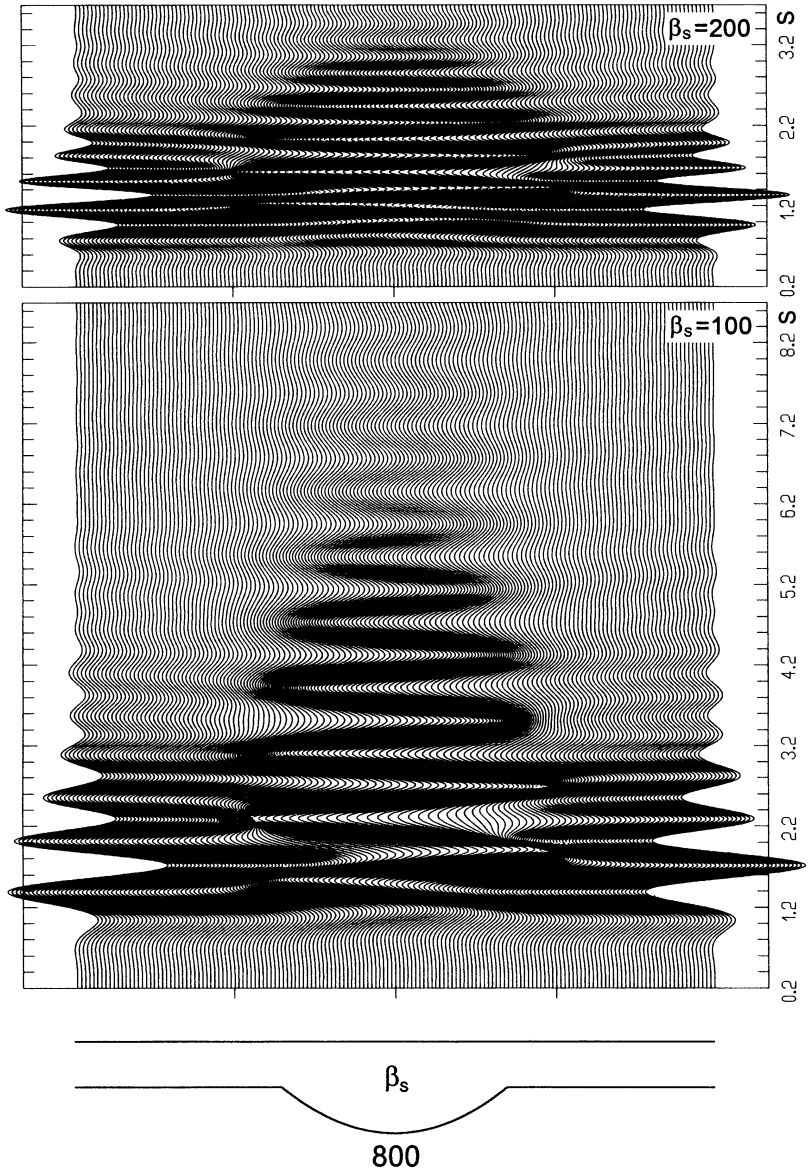

Figure 11. Time-domain representation of the fundamental modes of a 2D resonance due to a simple trough at the bottom of the horizontal surface layer in both the higher- and lower-contrast cases. The Gabor wavelets with parameters $\gamma = 4, f_p = 1.23$ Hz, $\psi = \pi/2$ and $\gamma = 6.5, f_p = 2.44$ Hz, $\psi = \pi/2$, respectively, were used as input signals.

ing resonant frequencies) may be "comparably dangerous" due to close maximum time-domain differential motions and that (2) a 2D resonance with significant spectral amplification and differential motion can arise in a simple trough at the bottom of the horizontal surface sedimentary layer.

Acknowledgments

We thank Michel Bouchon and two anonymous reviewers for critical reading of the manuscript, valuable comments, and suggestions that helped us to improve the article. We also thank Jose A. Rial for a useful discussion. This work was supported by NATO Linkage Grant ENVIR.LG 940714 and by Grant Number 2/1064/95, Grant Agency for Science, Slovak Academy of Sciences.

References

Bard, P.-Y. and M. Bouchon (1985). The two-dimensional resonance of sediment-filled valleys, *Bull. Seism. Soc. Am.* **75,** 519–541.

Bard, P.-Y. and J.-C. Gariel (1986). The seismic response of 2D sedimentary deposits with large vertical gradients, *Bull. Seism. Soc. Am.* **76,** 343–366.

Emmerich, H. and M. Korn (1987). Incorporation of attenuation into time-domain computations of seismic wave fields, *Geophysics* **52,** 1252–1264.

Jiang, T. and E. Kuribayashi (1988). The three-dimensional resonance of axisymmetric sediment-fields, *Soils Foundations* **28,** 130–146.

King, J. L. and B. E. Tucker (1984). Observed variations of earthquake motion across a sediment-filled valley, *Bull. Seism. Soc. Am.* **74,** 137–151.

Ling, H. and J. A. Rial (1990). Elastic eigenmodes in resonant 2D sedimentary basins of arbitrary shape, *EOS* **71,** 1459.

Ling, H. and J. A. Rial (1994). Asymptotic analysis of SH-wave modes in geologic resonators (sedimentary basins) of non-separable geometry, *Wave Motion* **19,** 245–270.

Moczo, P. and P.-Y. Bard (1993). Wave diffraction, amplification and differential motion near strong lateral discontinuities, *Bull. Seism. Soc. Am.* **83,** 85–106.

Moczo, P., A. Rovelli, P. Labák, and L. Malagnini (1995). Seismic response

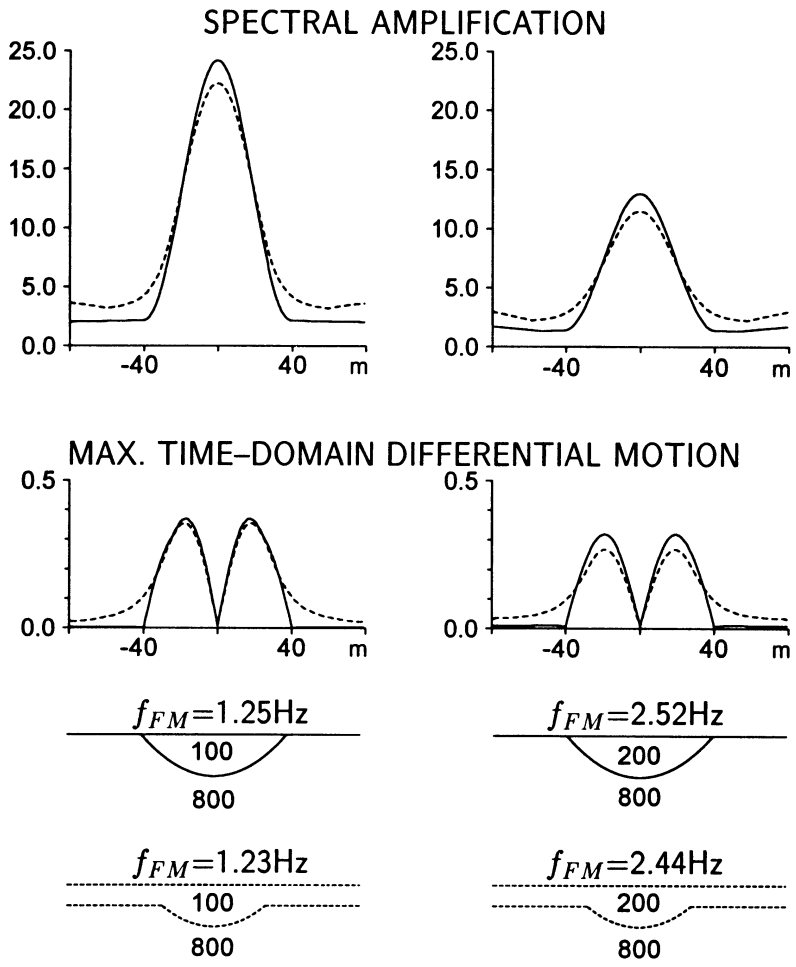

Figure 12. Comparison of the spectral amplifications and the maximum time-domain differential motions related to the fundamental modes of a 2D resonance in the closed valley and in the trough at the bottom of the horizontal surface layer in both the higher- and lower-contrast cases. The values of the differential motion have to be multiplied by 10^{-2} to be scaled for a maximum basement displacement of 1 cm.

of the geologic structure underlying Roman Colosseum and a 2D resonance of a sediment valley, *Annali Geofisica* **XXXVIII,** no. 5–6, 939–956.

Mossessian, T. K. and M. Dravinski (1990). Resonance motion of three-dimensional Alluvial Basins, in *Proc. of the 4th U.S. National Conference on Earthquake Engineering* **1,** 525–534.

Ohori, M., K. Koketsu, and T. Minami (1990). Seismic response analyses of sediment-filled valley due to incident plane wave by three-dimensional Aki-Larner method, *Bull. Earthquake Res. Inst. Tokyo Univ.* **65,** 433–463.

Reynolds, A. C. (1978). Boundary conditions for the numerical solution of wave propagation problems, *Geophysics* **43,** 1099–1110.

Rial, J. A. (1989). Seismic wave resonances in 3D sedimentary basins, *Geophys. J. Int.* **99,** 81–90.

Rial, J. A. and H. Ling (1992). Theoretical estimation of the eigen-frequencies of 2-D resonant sedimentary basins: numerical computations and analytic approximations to the elastic problem, *Bull. Seism. Soc. Am.* **82,** 2350–2367.

Rial, J. A., N. G. Saltzman, and H. Ling (1991). Computation of eigenmodes of resonant sedimentary basins of arbitrary shape by semi-classical and variational methods, *Wave Motion* **14,** 377–398.

Rial, J. A., N. G. Saltzman, and H. Ling (1992). Earthquake-induced resonance in sedimentary basins, *Am. Sci.* Nov–Dec, 566–578.

Tucker, B. E. and J. L. King (1984). Dependence of sediment-filled valley response on input amplitude and valley properties, *Bull. Seism. Soc. Am.* **74,** 153–165.

Wirgin, A. (1995). Resonant response of a soft semi-circular cylindrical basin to an SH seismic wave, *Bull. Seism. Soc. Am.* **85,** 285–299.

Zhou, T. and M. Dravinski (1994). Resonance prediction of deep sediment valleys through an eigenvalue method, *Geophys. J. Int.* **117,** 749–762.

Geophysical Institute
Slovak Academy of Sciences
Dúbravská cesta
842 28 Bratislava
Slovak Republic
(P.M., P.L., J.K.)

Department of Physics
University of Alberta
Edmonton, Alberta
T6G 2J1 Canada
(F.H.)

Manuscript received 18 October 1995.